Surgical Oncology 33 (2020) 145–157

Contents lists available at ScienceDirect

Surgical Oncology

journal homepage: http://www.elsevier.com/locate/suronc

Radiofrequency ablation with four electrodes as a building block for matrix radiofrequency ablation: *Ex vivo* liver experiments and finite element method modelling. Influence of electric and activation mode on coagulation size and geometry

Stefaan Mulier [a,b], Ricardo Possebon [c], Yansheng Jiang [b], Jacques Jamart [d], Chong Wang [c], Yi Miao [e], Tongfu Yu [e], Kuirong Jiang [e], Yuanbo Feng [b], Guy Marchal [b], Luc Michel [f], Yicheng Ni [b,*]

[a] Department of Surgery, Delta Hospital, CHIREC Cancer Institute, Triomflaan 201, 1160, Brussels, Belgium
[b] Department of Radiology, Gasthuisberg University Hospital, Herestraat 49, 3000, Leuven, Belgium
[c] Alegrete Technology Center, Federal University of Pampa, Av. Tiarajú 810, Ipirabuitã, CEP 97546-550, Alegrete, Rio Grande do Sul, Brazil
[d] Department of Biostatistics, Mont-Godinne University Hospital, Avenue du Dr. Thérasse 1, 5530, Yvoir, Belgium
[e] Department of Surgery and Radiology, First Hospital of Nanjing Medical University, Guangzhou Road No 300, 210029, Nanjing, China
[f] Department of Surgery, Mont-Godinne University Hospital, Avenue du Dr. Thérasse 1, 5530, Yvoir, Belgium

ARTICLE INFO

Keywords:
Radiofrequency ablation
Matrix
Bipolar
Liver
Finite element method

ABSTRACT

Purpose: Radiofrequency ablation (RFA) is increasingly being used to treat unresectable liver tumors. Complete ablation of the tumor and a safety margin is necessary to prevent local recurrence. With current electrodes, size and shape of the ablation zone are highly variable leading to unsatisfactory local recurrence rates, especially for tumors >3 cm. In order to improve predictability, we recently developed a system with four simple electrodes with complete ablation in between the electrodes. This rather small but reliable ablation zone is considered as a building block for matrix radiofrequency ablation (MRFA). In the current study we explored the influence of the electric mode (monopolar or bipolar) and the activation mode (consecutive, simultaneous or switching) on the size and geometry of the ablation zone.

Materials and methods: The four electrode system was applied in ex vivo bovine liver. The electric and the activation mode were changed one by one, using constant power of 50 W in all experiments. Size and geometry of the ablation zone were measured. Finite element method (FEM) modelling of the experiment was performed.

Results: In ex vivo liver, a complete and predictable coagulation zone of a 3 × 2 × 2 cm block was obtained most efficiently in the bipolar simultaneous mode due to the combination of the higher heating efficacy of the bipolar mode and the lower impedance by the simultaneous activation of four electrodes, as supported by the FEM simulation.

Conclusions: In ex vivo liver, the four electrode system used in a bipolar simultaneous mode offers the best perspectives as building block for MRFA. These results should be confirmed by in vivo experiments.

1. Introduction

Radiofrequency ablation (RFA) is increasingly being applied to obtain local control of unresectable primary [1] and secondary [2] liver tumors.

In order to prevent local recurrence, a complete coagulation of the tumor including a 10 mm safety margin is necessary for small (<3 cm) [3] and medium size (3–5 cm) [4] hepatocellular carcinomas (HCC) as well as for colorectal liver metastases (CRLM) [5]. The first experiments with RF ablation on liver tissue were performed with plain metal electrodes. The ablation diameter was very limited, due to a rapid rise in electric impedance with current shut-off [6]. Since 1992, new RFA

* Corresponding author. Department of Radiology, University Hospital Gasthuisberg, Theragnostic Laboratory, Department of Imaging & Pathology, Faculty of Medicine, KU Leuven, Herestraat 49, B-3000, Leuven, Belgium..
E-mail addresses: yicheng.ni@kuleuven.be, yicheng.ni@med.kuleuven.be (Y. Ni).

https://doi.org/10.1016/j.suronc.2020.02.005
Received 24 May 2019; Accepted 7 February 2020
Available online 10 February 2020
0960-7404/

electrodes with ingenious designs (wet, cooled, expandable, bipolar, cooled-wet) and combinations of these designs [7], more powerful generators [8] and improved treatment protocols such as pulsed RFA [9], stepwise deployment of expandable electrodes [10], stepwise increase of current [11,12] and rapid switching between multiple electrodes [13] have been introduced to successfully *increase mean ablation diameter*, but unfortunately attention to *improve predictability of the size and the shape of the ablation zone* has lagged behind. Ablation zones are often smaller or larger than expected and less symmetrical, less spherical and less regular than desired [12,14–50]. A standard deviation of the ablation diameter, especially the transverse diameter, of 0.5–1 cm is very common [51]. The *high variability of size and shape* of the ablation zone may contribute to incomplete ablation and local recurrence after RFA of liver tumors.

Despite technical improvements in RFA technology, *local recurrence rates* after RFA of liver tumors remain unsatisfactory, especially for tumors >3 cm, even in the most recent clinical trials. A review of all studies published between January 1st, 2013 and May 1st, 2019, revealed that local recurrence rates after a follow-up of ≥2 years after RFA of HCC <3 cm are highly variable, ranging from between 2.9 and 10% [52–59], between 10 and 20% [57–70], between 20 and 46.6% [3,56,71–84] up to between 73.3% and 76.3% [85,86]. Local recurrence rates after RFA of HCC 3–5 cm vary between 7.1 and 59.4% [4,52–54,60,64,87]. Local recurrence rates after RFA of HCC >5 cm vary between 18.7 and 48.4% [87,88].

Local recurrence rates after RFA of CRLM <3 cm range from between 2.9 and 10% [89–95] to between 15 and 18.2% [96–98] up to 40–58.3% [99–102]. Local recurrence rates after RFA of CRLM between 3 and 5 cm vary between 19.6% and 32.0% [89–91,98] up to 69.6% [99]. Local recurrence rates after RFA of CRLM >5 cm vary between 30.8% and 71.4% [90,98].

Incomplete ablation of liver tumors not only leads to local recurrence but also renders a tumor more aggressive than before. *Aggressive growth of residual tumor cells* has been shown after insufficient ablation of both HCC [103] and CRLM [104].

Incomplete ablation or local recurrence after RFA of HCC [105] or CRLM [106] is associated with worse overall survival in most studies.

At present, RFA is recommended for the treatment of HCC in case of non perivascular lesions ≤2 cm because of equivalent local control and survival rates with less morbidity compared to hepatic resection, while surgery remains the first treatment option for larger and for perivascular lesions because of higher local recurrence rates and decreased survival after RFA [107]. RFA is beneficial for the treatment of *unresectable CRLM* ≤ 3 cm [108–110], while surgical resection continues to be the gold standard for *resectable CRLM* of any size because of higher local recurrence rates and decreased survival after RFA [109].

So in fact, there is more than a so-called '3-cm problem' [111] to be solved or a '3 cm-barrier' [112] to be broken for hepatic RFA technology: local tumor control should be improved for *both* small (≤3 cm) and large (3–5 cm and >5 cm) tumors before RFA can replace surgery for liver tumors.

The *high variability of size and shape of the ablation zone* may also contribute to collateral damage and complications due to larger than expected ablation such as hepatic failure, biliary damage, perihepatic visceral burns or burns to the diaphragm [15,46,56,113–116].

In conclusion, there is a definite need to improve the technique of hepatic RFA in order to obtain a (1) predictable, (2) reliable and (3) safe ablation zone. *Predictable* means that the size and shape of the ablation zone can be predicted with great precision before starting the ablation by choosing a certain electrode (system) and by applying a certain ablation protocol (duration, energy input, …). Size and shape should not depend on the nature of the tumor nor on the features of the surrounding liver parenchyma and should not vary between operating physicians. *Reliable* means that all tissue within the ablation zone is completely ablated without gaps or indentations. *Safe* means that no tissue is ablated outside the intended zone of the tumor and a 10 mm safety margin.

To improve predictability, reliability and safety of liver RFA, we are working on the development of matrix radiofrequency ablation (MRFA) in which the whole tumor volume and the safety margin is contained within a cage of x times y parallel electrodes [51]. The smallest 'building block' for MRFA is a cluster of 2 × 2 parallel simple needle electrodes [51,117]. Our previous work has shown that complete ablation within the mechanical boundaries of the electrodes with minimal ablation outside was obtained in a very reproducible way in ex vivo bovine liver using 2 × 2 parallel simple needle electrodes in a bipolar simultaneous mode with a length of 3 cm, a diameter of 1.8 mm, an interelectrode distance of 2 cm, a power of 50 W and an ablation duration of 10 min or until current shut-off due to impedance rise [51,117]. The rectangular shape of the ablation closely matches the rectangular shape of the volume in between the active parts of the 2 × 2 electrodes with limited ablation outside (maximal ablation margin outside the electrodes of 7.1 ± 2.2 mm) [117]. Variability of ablation size, expressed either as SD (standard deviation) or as CV (coefficient of variation = standard deviation/mean diameter) was limited and smaller than for many currently available electrodes, both in the axial and the transverse plane [51].

By adding up these rather small but very reliable rectangular ablation zones, large ablation zones of any size or shape could be performed.

The aim of the current study was to further explore the performances of the 2 × 2 electrode system in ex vivo liver. We used the same parameters as in the optimal setting found in the previous studies except that we varied the electric mode (unipolar or bipolar) and the activation mode (consecutive, simultaneous or switching) [7]. Size, geometry and completeness of the ablation zone were measured. In a second step, the experiments were simulated by finite element method (FEM) modelling to help us interpret the experimental results.

2. Materials and methods

The experimental set-up and the measurement of lesion size have been described in detail before [51,117]. For the experiments in the monopolar mode, a 15 × 7.5 cm ground pad (dispersive electrode) was put under the liver, with the nearest edge of the plate shifted 10 cm to the left of the center in between the 4 electrodes.

2.1. Ablation protocol

Six experiments, each consisting of six ablations, have been performed (Fig. 1).

1. monopolar consecutive
2. monopolar simultaneous
3. monopolar switching
4. bipolar consecutive
5. bipolar simultaneous
6. bipolar switching

Monopolar indicates a current flow between the electrodes and the ground pad.

Bipolar indicates a current flow between two (pairs of) electrodes without ground pad.

Monopolar consecutive indicates that the ablation is started with the first electrode and continued during 10 min or until current shut-off due to impedance rise. This is repeated without interval with the second electrode, then with the third and finally with the fourth electrode.

Monopolar simultaneous indicates that the four electrodes are activated simultaneously during 10 min or until current shut-off due to impedance rise.

Monopolar switching indicates that the first electrode is activated for 1 s, followed without interval by the second electrode, the third and finally the fourth electrode. This activation cycle is continuously repeated during 10 min or until current shut-off due to impedance rise.

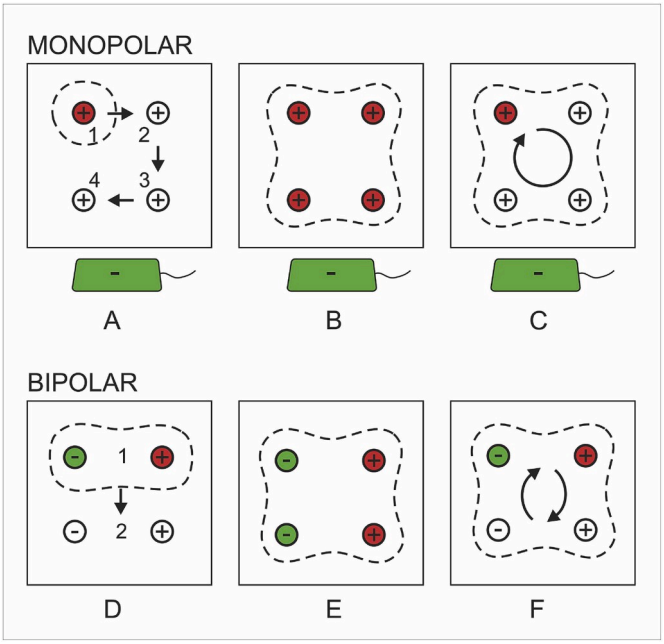

Fig. 1. Experimental set-up, schematic representation of electric and activation modes.
A. monopolar consecutive
B. monopolar simultaneous
C. monopolar switching
D. bipolar consecutive
E. bipolar simultaneous
F. bipolar switching.

Bipolar consecutive indicates that the ablation is started with the first pair of electrodes and continued during 10 min or until current shut-off due to impedance rise. This is repeated without interval with the second pair of electrodes.

Bipolar simultaneous indicates that the two electrode pairs are activated simultaneously during 10 min or until current shut-off due to impedance rise.

Bipolar switching indicates that the first electrode pair is activated for 1 s, followed without interval by the second electrode pair. This activation cycle is continuously repeated during 10 min or until current shut-off due to impedance rise.

Complete coagulation means that the whole volume circumscribed by the active parts of the four electrodes was completely coagulated as measured in both planes. Complete coagulation was given a score 1, incomplete (even 90%) coagulation a score 0, since obtaining a 100% reliable complete coagulation was a key objective in this study.

The minimal axial diameter was defined as the diameter of the ablation zone at the *central axis* between the 4 electrodes [117].

Heating efficacy was calculated by FEM modelling and was defined as the amount of energy delivered in the volume *in between the active parts of the four electrodes* divided by the total amount of energy delivered, expressed as a percentage.

2.2. Statistical analysis

Numerical data were reported as mean ± standard deviation. A multivariate analysis of data was carried out to take into account the simultaneous influence of the six combinations of electric mode and activation mode (as analysed in this paper), interelectrode distance (as analysed in a first paper [117]), power, duration, electrode diameter and pattern (as analysed in a second paper [51].

Duration of coagulation, end temperature, time and coagulation speed (numerical data) were analysed by linear regression, and completeness of coagulation (dichotomous data) by logistic regression. Regression analysis of repeated measures using generalized estimating equation (GEE) was performed to study the values of temperature, impedance and current at every minute. Results between two groups were compared with unpaired *t*-test with Welch's correction (Table 4). Results between more than two groups were compared with one way ANOVA following Bonferroni's test (Table 2, Table 5, Table 6). A P value less than 0.05 was considered as statistically significant. Statistical analysis was performed using SPSS 15.0 statistical software (SPSS Inc., Chicago, IL, USA).

2.3. Finite element method analysis

In order to further understand the influence of the aforementioned parameters on coagulation size and geometry, we performed a finite element method (FEM) modelling using RAFEM-3 which has been described in detail in the supplemental data.

3. Results

3.1. Finite element method modelling

The experimentally measured and numerically predicted transient temperatures matched closely (Fig. 2, Fig. 3). The 60 °C isotherms calculated by FEM modelling were similar in shape to the borders of the ablation zones observed in our experiments (Fig. 4, Fig. 5). The minimal axial diameter as measured after each experiment was predicted well by FEM modelling except for the very incomplete ablations in the monopolar and bipolar consecutive modes (Table 1).

3.2. Monopolar consecutive mode

In the monopolar consecutive mode, impedance at the start was very high (136 ± 7.7 Ohm) (Table 2). Current shut-off due to impedance rise occurred early: 3.82 ± 1.60 min after activation of the first electrode. Duration of the total experiment (4 consecutive activations until current shut-off) was 10.85 ± 2.34 min. End temperature was limited to 52.0 ± 4.6 °C. Coagulation was always incomplete, ranging from four individual coagulations around each electrode without any fusion to a cloverleaf shape coagulation consisting of four individual coagulations with

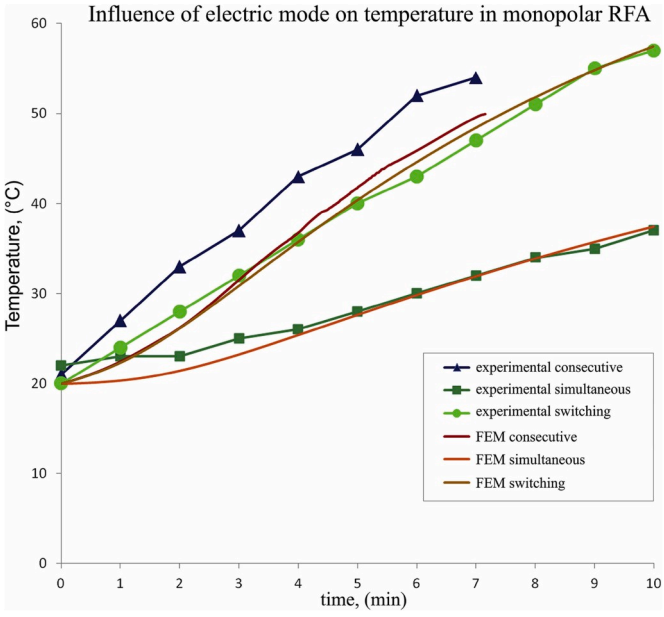

Fig. 2. Monopolar RFA: influence of electric mode on temperature and comparison of experimental and simulation values.

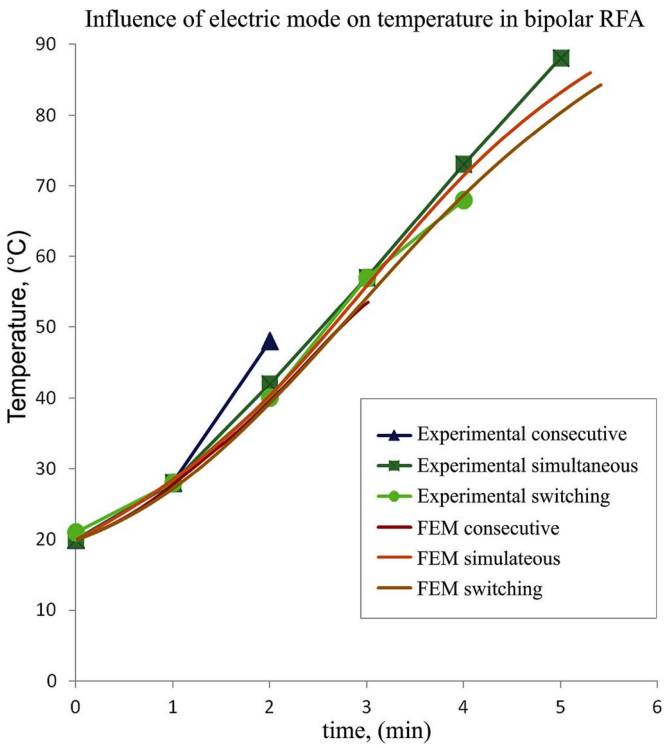

Fig. 3. Bipolar RFA: influence of electric mode on temperature and comparison of experimental an simulation values.

limited coagulation in between (Fig. 4A).

FEM modelling of the electric field squared (hereafter called electric field throughout the manuscript for simplicity) showed that the electric field developed in a concentric way around each electrode, be it with some deviation of the electric field to the left of the electrodes, i.e. in the direction of the ground pad (Fig. 6A). FEM modelling of temperature distribution showed four coagulations around each electrode with incomplete fusion between them (Fig. 5A). Maximal temperatures were high (>100 °C) and concentrated around the electrodes.

3.3. Monopolar simultaneous mode

In the monopolar simultaneous mode, temperature hardly rose, with a temperature of 32.2 ± 5.8 °C after 10 min (Table 2, Fig. 2). Coagulation was very weak and limited to the electrodes that were nearest to the ground pad (Fig. 4B).

FEM modelling showed that the maximal intensity of the electric field was much lower (<3000 V/m) than in the other modes (Fig. 6B). The size of the electric field >1000 V/m was much smaller than in the monopolar consecutive mode. The electric field was close to zero in the volume in between the four electrodes. The field was distributed in a centrifugal way, away from the center towards the outer side of each electrode. Finally, the field was deviated to the left of the electrodes, i.e. in the direction of the ground pad. The simulation of the temperature distribution followed the same pattern: maximal temperatures were low (<60 °C) and heating was limited to the electrodes that were nearest to the ground pad (Fig. 5B).

3.4. Monopolar switching mode

In the monopolar switching mode, temperature went up slowly, with a temperature of 52.2 ± 7.4 °C after 10 min (Table 2, Fig. 2). Coagulation was complete in the transverse plane in 4 out of 6 experiments but incomplete in the axial plane in 5 out of 6 experiments due to small to moderate sized uncoagulated areas at the proximal and the distal end of the axis between the four electrodes (Fig. 4C).

FEM modelling showed that the electric field around a single activated electrode was very similar in shape, size and intensity to the field in the monopolar consecutive mode (Fig. 6C). The electric field developed in a nearly concentric way around each electrode, although with some deviation of the electric field to the left of the electrodes, i.e. in the direction of the ground pad. The simulation of the temperature distribution showed higher maximal temperatures (70–100 °C) (Fig. 5C). In contrast to the monopolar consecutive mode however, there was a nice fusion of coagulation zones in between the four electrodes. The coagulation zone based on the 60 °C isotherm was nearly symmetrical. Furthermore, it was complete, in contrast to 5 out of 6 ex vivo experiments.

3.5. Bipolar consecutive mode

In the bipolar consecutive mode, temperature went up quickly but current shut-off due to impedance rise occurred very early: 1.15 ± 0.12 min after activation of the first electrode (Table 2, Fig. 3). Duration of the total experiment (2 consecutive activations until current shut-off) was only 2.30 ± 0.14 min. End temperature was 57.3 ± 6.4 °C. Coagulation was always incomplete (Fig. 4D).

FEM modelling of the electric field showed that the electric field developed symmetrically around and in between both electrodes (Fig. 6D). The size of the electric field >1000 V/m was about twice the size of the electric field >1000 V/m in the monopolar consecutive mode. FEM modelling of end temperature distribution showed four individual coagulations as determined by the 60 °C isotherm around each electrode (Fig. 5D). Maximal temperatures were high (>100 °C) and concentrated around the electrodes. Size and shape of the coagulation as determined by the 60 °C isotherm closely resembled the experimental findings ex vivo.

3.6. Bipolar simultaneous mode

In the bipolar simultaneous mode, temperature went up very smoothly (Fig. 3). Impedance first decreased during the first 3 min, then increased from 4 min on until a sudden impedance rise occurred (Table 2). With constant power output of 50 W, current first increased during the first 3 min, and then decreased from 4 min on until current shut-off. The ablation process took 5.30 ± 0.70 min. End temperature was 77.7 ± 12.4 °C. Coagulation was always complete in both the axial and the transverse plane (Fig. 4E). The coagulation zone was remarkably homogenous, without the typical carbonization which is often seen in RFA using other electrodes. The rectangular shape of the coagulation closely matched the rectangular shape of the volume in between the active parts of the four electrodes, extending 2.9 ± 2.1 mm beyond this volume in the axial plane and 6.4 ± 1.9 mm in the transverse plane (calculated on both the minimal and the maximal measurement in each plane).

FEM modelling showed a high and symmetric electric field >1000 V/m in the square determined by the four electrodes and a limited electric field outside this area (Fig. 6E). This resulted in a complete coagulation as determined by the 60 °C isotherm with very efficient and homogenous heating in between the electrodes (with temperatures above 80 °C in nearly the whole volume) with only limited heating outside (Fig. 5E). Size and shape of the coagulation as determined by the 60 °C isotherm closely resembled the experimental findings ex vivo.

3.7. Bipolar switching mode

In the bipolar switching mode, temperature went up quickly up till 53.2 ± 16.6 °C, but current was prematurely shut-off due to impedance rise after 4 min (Table 2, Fig. 3).

FEM modelling of the electric field showed that the electric field developed symmetrically around and in between both electrodes

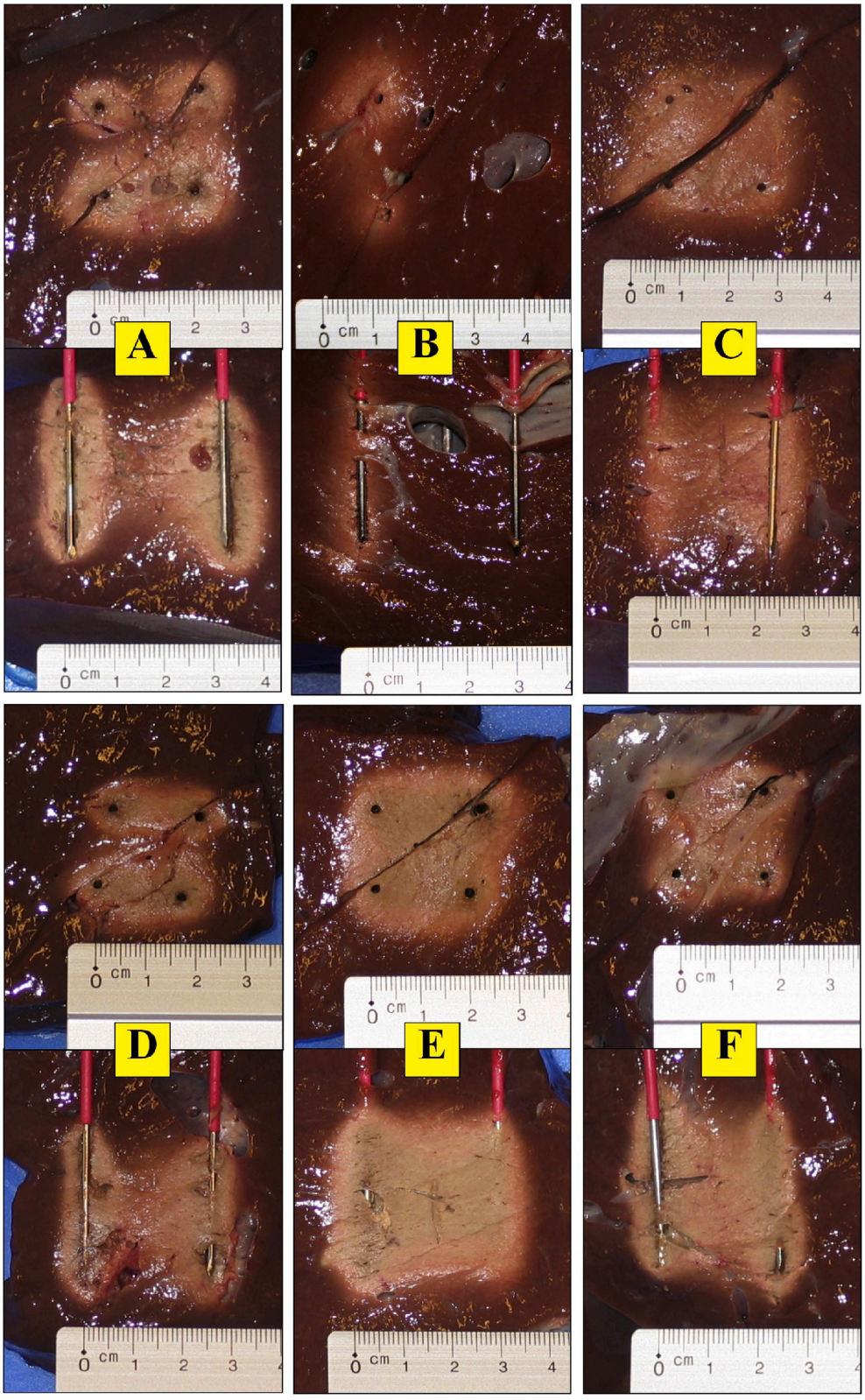

Fig. 4. Ex vivo bovine liver experiments: influence of electric and activation mode on coagulation zone in transverse and axial plane
A. monopolar consecutive.
B. monopolar simultaneous.
C. monopolar switching.
D. bipolar consecutive.
E. bipolar simultaneous.
F. bipolar switching.

(Fig. 6F). The size of the electric field >1000 V/m was about twice the size of the electric field >1000 V/m in the monopolar switching mode. FEM modelling of end temperature distribution showed a complete coagulation in between the four electrodes (Fig. 5F). Temperatures were lower than in the bipolar simultaneous mode, with a larger waist in the axial plane, although this didn't compromise completeness of coagulation based on the 60 °C isotherm. In contrast to the FEM modelling, coagulation was incomplete in 4 out of 6 ex vivo experiments, mainly because the waist phenomenon in the axial plane was more pronounced ex vivo (Fig. 4F).

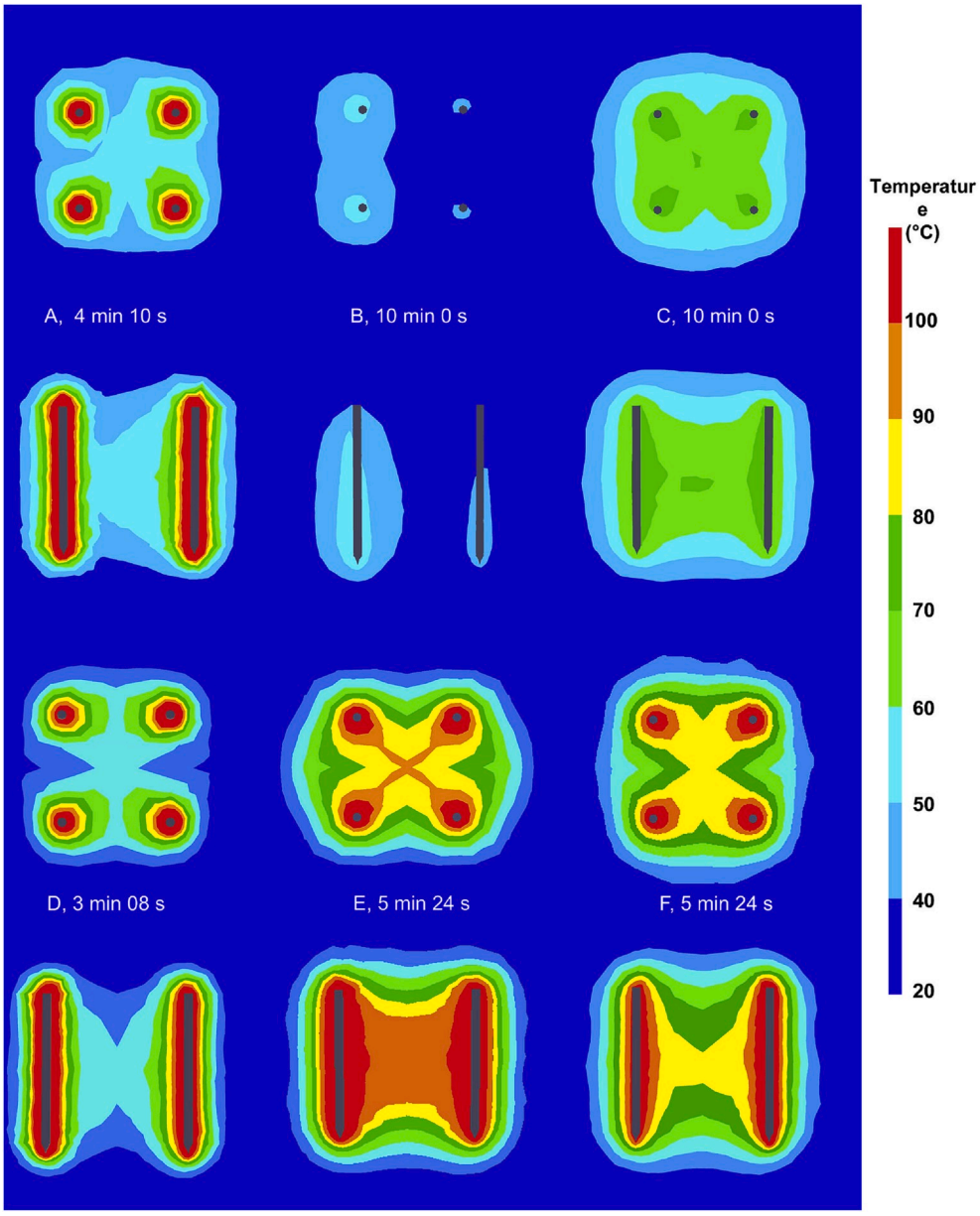

Fig. 5. FEM modelling with RAFEM-3: influence of electric and activation mode on temperature distribution (°C) in transverse and axial plane *at the end* of each experiment
A. monopolar consecutive.
B. monopolar simultaneous.
C. monopolar switching.
D. bipolar consecutive.
E. bipolar simultaneous.
F. bipolar switching.

Table 1
Comparison of minimal axial diameter of the ablation zone in ex vivo bovine liver experiments and in FEM modelling.

electric mode (EM)	monopolar	monopolar	monopolar	bipolar	bipolar	bipolar
activation mode (AM)	consecutive	simultaneous	switching	consecutive	simultaneous	switching
ex vivo *(mm)*	*6 ± 9.4*	*0 ± 0*	*19.7 ± 11.6*	*8.2 ± 9.4*	*35.5 ± 1.2*	*26.7 ± 3.1*
FEM (mm)	*0*	*0*	*22*	*0*	*34*	*29*

The minimal axial diameter was defined as the the diameter of the ablation zone at the central axis between the 4 electrodes.
The 60 °C isotherm was used to define the borders of the ablation zone by FEM modelling.

3.8. Comparison between all 6 combinations of modes

Current intensity and impedance at the start, peak current, end temperature, time until current shut-off, complete coagulation score and heating efficacy were significantly different for each of the six combinations of modes (Table 2, Table 3).

The bipolar simultaneous mode had the highest current and the lowest impedance at the start and the highest current peak (Table 2). It was the only mode that allowed heating ≥60 °C at the measuring point in the center of the plane created by the tips of the four electrodes, as well as complete coagulation in the axial and the transverse plane in all experiments (Table 2, Fig. 3). Heating efficacy was largest for the bipolar simultaneous mode and lowest for the monopolar simultaneous mode (Table 3).

3.9. Bipolar versus monopolar mode

In the bipolar mode, impedance at the start and time until shut-off

Table 2
Outcome of the ex vivo bovine liver experiments: comparison of the six combinations of electric and activation modes.

electric mode (EM)	monopolar	monopolar	monopolar	bipolar	bipolar	bipolar	p
activation mode (AM)	consecutive	simultaneous	switching	consecutive	simultaneous	switching	
n activated electrodes	1	4	1	2	4	2	
impedance (start) (Ohm)	136 ± 7.7	81 ± 21.2	154.7 ± 23.4	125.7 ± 28.1	73 ± 4.6	135.2 ± 7.7	$p < 0.001$
current (start) (cAmp)	62.8 ± 1.8	82.2 ± 11.7	58 ± 4.5	71.5 ± 5.4	87.7 ± 3.1	66.8 ± 3.1	$p < 0.001$
current (peak) (cAmp)	72.7 ± 1.8	87 ± 14.2	66.5 ± 5.8	84.2 ± 2.6	118.3 ± 5.3	86.2 ± 4.5	$p < 0.001$
end temperature (°C)	52 ± 4.6	32.2 ± 5.8	52.2 ± 7.4	57.3 ± 6.4	77.7 ± 12.4	53.2 ± 16.6	$p < 0.001$
time until shut-off (min)	3.82 ± 1.60	10 ± 0.00	10 ± 0.00	1.15 ± 0.12	5,30 ± 0.70	3.46 ± 0.42	$p < 0.0001$
complete coagulation score	0	0	0.17	0	1.00	0.33	$p < 0.001$

were lower while current at the start, peak current, end temperature and complete coagulation score were higher (Table 4). Heating efficacy was more than twice as high for all bipolar modes (Table 3).

3.10. Consecutive versus simultaneous versus switching mode

In the simultaneous mode, impedance at the start was lower while current at the start, peak current, time until shut-off and complete coagulation score were higher when compared to the consecutive and the switching mode (Table 5).

3.11. Number of electrodes activated at the same time

With increasing number of electrodes activated at the same time, impedance at the start was lower while current at the start, peak current and complete coagulation score were higher (Table 6).

4. Discussion

Multiple electrodes systems for RFA can be used in two *electric modes*: unipolar or bipolar and in three *activation modes*: consecutive, simultaneous and switching [7].

We recently described an electrode system consisting of four parallel 3 cm simple needle electrodes that allowed a reliable and predictable ablation zone in ex vivo liver in the *bipolar simultaneous mode* [51,117]. In the current study we explored the influence of changing the electric mode and the activation mode on the size and geometry of the ablation zone.

4.1. Monopolar versus bipolar mode

(1) In the monopolar *simultaneous* mode, the Faraday cage effect [118] occurs: since all four electrodes have the same polarity, the electric field is deformed and pushed outwards, with almost no current flowing and almost no coagulation in the target zone between the electrodes (Fig. 4B).
(2) In *all three* monopolar modes heating of the target volume is less efficient than in the bipolar mode because a major part of the energy is lost in the tissue between the electrodes and the ground pad. While this principle seems intuitively logical, it has to our best knowledge not been quantified before. Using the newly introduced definition of heating efficacy, FEM was able to show that energy delivery in the target volume was more than twice as efficient in the bipolar than in the monopolar mode (Table 3).
(3) In all monopolar modes, electric field, thermal distribution and coagulation were asymmetric and deviated towards the ground pad. This asymmetric coagulation observed with monopolar electrodes may be of concern for hepatic RFA performed by laparotomy or by laparoscopy. Current between the electrodes and the ground pad will flow through the path with the least electric resistance. With a surgical approach, current will preferentially flow centrally towards the liver hilum which is much more in (electric) contact with the rest of the body than the liver capsule which is exposed to the air or to CO_2. This may, at least in theory, cause an unwanted asymmetric coagulation in the direction of the hilum. This phenomenon may be less prominent in percutaneous RFA, at least when no artificial pneumoperitoneum is created.

In summary, three undesirable effects of monopolar RFA have been confirmed or identified: (1) the Faraday cage effect, (2) the lower heating efficacy in the target volume, (3) asymmetric coagulation towards the ground pad.

In the bipolar modes, the above mentioned undesirable effects were not found. The electric field was stronger and more concentrated, leading to a higher heating efficacy in the target volume with faster heating and a higher complete coagulation score. Faster heating in bipolar RFA has been shown to partially [43,119–122] or completely [123] reduce the heat-sink effect in proximity of large vessels as seen in monopolar RFA, with results approaching those for fast heating during microwave ablation [121].

4.2. Consecutive versus simultaneous versus switching mode

In the ex vivo experiments, the simultaneous activation mode was superior to the consecutive and the switching mode in combination with the bipolar electric mode. The double number of electrodes activated at the same time in the simultaneous mode versus the consecutive and the switching mode (4 versus 2 and 2) decreased impedance at the start by 42–46%, allowing a higher current for a longer time, resulting in a higher end temperature and a higher complete coagulation score (Table 2). We are not aware of similar comparative experiments in the bipolar mode. The superiority of the simultaneous (bipolar) mode over the switching (bipolar) mode is new and in contrast to the usual superiority of the switching mode over the simultaneous mode in experiments with monopolar electrodes [13,124–127].

4.3. Number of electrodes activated at the same time

Impedance at the start significantly dropped when increasing the number of electrodes that were activated at the same time, especially when increasing from 2 to 4 (Table 6).

The lower impedance allowed maintaining a higher current for a longer time before the occurrence of current shut-off and resulted in the highest complete coagulation score.

We believe that the 'secret' of the better performance of the bipolar simultaneous mode compared to the 5 other modes lies in the combination of the higher heating efficacy of the bipolar mode and the lower impedance by the simultaneous activation of four electrodes.

4.4. Bipolar simultaneous mode

The bipolar simultaneous mode was the most efficient combination to provide a complete coagulation zone of a 3 × 2 × 2 cm block. The good results are due to the combination of the higher heating efficacy of the bipolar mode and the lower impedance by the simultaneous

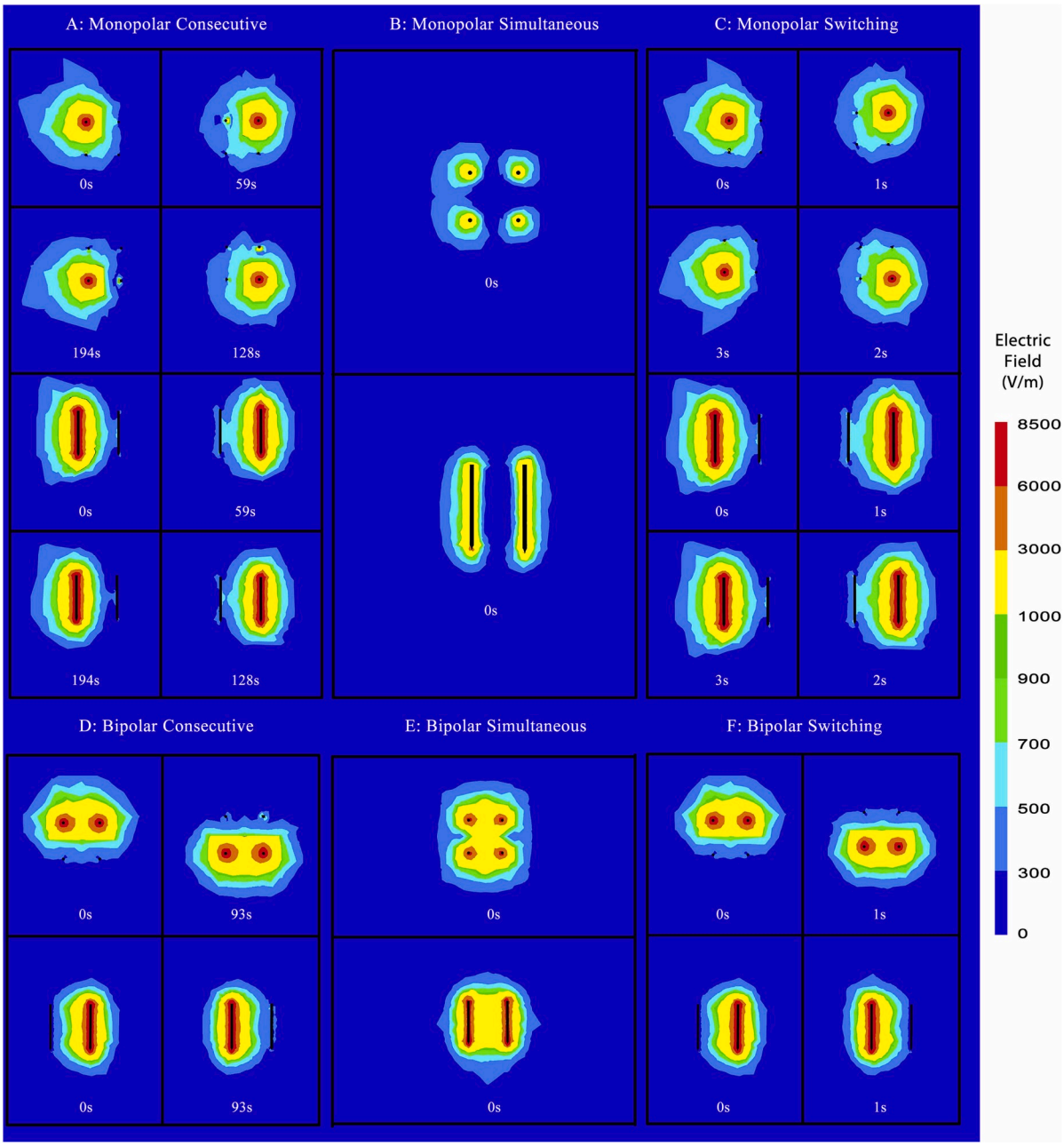

Fig. 6. FEM modelling with RAFEM-3: influence of electric and activation mode on electric field squared (V/m) in transverse and axial plane *at the start* of each (part of) experiment
A. monopolar consecutive
B. monopolar simultaneous
C. monopolar switching
D. bipolar consecutive
E. bipolar simultaneous
F. bipolar switching.

Table 3
Comparison of heating efficacy according to electric and activation mode.

electric mode (EM)	monopolar	monopolar	monopolar	bipolar	bipolar	bipolar
activation mode (AM)	consecutive	simultaneous	switching	consecutive	simultaneous	switching
heating efficacy (%)	*9.53*	*3.41*	*9.89*	*22.93*	*25.37*	*23.46*

Heating efficacy as calculated by FEM modelling is defined as the amount of energy delivered in the target volume between the active parts of the four electrodes divided by the total amount of energy delivered, expressed as a percentage.

Table 4
Outcome of the ex vivo bovine liver experiments: comparison of the two electric modes.

electric mode	monopolar	bipolar	p
impedance (start) (Ohm)	*123.9 ± 36.7*	*111.3 ± 32.4*	*NS*
current (start) (cAmp)	*67.7 ± 12.8*	*75.3 ± 9.9*	*p = 0.0064*
current (peak) (cAmp)	*75.1 ± 12.4*	*96.2 ± 16.6*	*p = 0.0022*
end temperature (°C)	*45.4 ± 11.2*	*62.7 ± 16.1*	*p = 0.0049*
time until shut-off (min)	*7.94 ± 3.12*	*3.31 ± 1.80*	*p < 0.0001*
complete coagulation score	*0.06*	*0.44*	*p = 0.0074*

Table 5
Outcome of the ex vivo bovine liver experiments: comparison of the three activation modes.

activation mode	consecutive	simultaneous	switching	p
impedance (start) (Ohm)	*130.8 ± 20.4*	*77.0 ± 15.2*	*144.9 ± 19.5*	*p < 0.0001*
current (start) (cAmp)	*67.2 ± 6.0*	*84.9 ± 8.7*	*62.4 ± 5.9*	*p < 0.0001*
current (peak) (cAmp)	*78.4 ± 6.4*	*102.7 ± 19.3*	*75.8 ± 11.9*	*p = 0.003*
end temperature (°C)	*54.7 ± 6.0*	*54.9 ± 25.5*	*52.7 ± 12.2*	*NS*
time until shut-off (min)	*2.48 ± 1.76*	*7.65 ± 2.50*	*6.73 ± 3.42*	*p = 0.0003*
complete coagulation score	*0*	*0.50*	*0.25*	*p = 0.021*

Table 6
Outcome of the ex vivo bovine liver experiments: comparison according to the number of electrodes activated at the same time.

n activated electrodes	1	2	4	p
combinations	monopolar consec/ switching	bipolar consec/ switching	monopolar/ bipolar simultaneous	
impedance (start) (Ohm)	*145.3 ± 19.2*	*130.4 ± 20.3*	*77 ± 15.2*	*p < 0.0001*
current (start) (cAmp)	*60.4 ± 4.1*	*69.2 ± 4.9*	*84.9 ± 8.7*	*p < 0.0001*
current (peak) (cAmp)	*69.1 ± 5.5*	*85.2 ± 3.7*	*102.7 ± 19.3*	*p = 0.0046*
end temperature (°C)	*52.1 ± 5.9*	*55.3 ± 12.2*	*54.9 ± 25.5*	*p = NS*
time until shut-off (min)	*6.91 ± 3.40*	*2.31 ± 1.24*	*7.65 ± 2.50*	*p < 0.0001*
complete coagulation score	*0.08*	*0.17*	*0.50*	*p = 0.049*

activation of four electrodes.

The boundaries of the coagulation zone were closely determined by the position of the electrodes, which enhances the *predictability of the shape* of the ablation.

The variability of the ablation size, expressed either as SD (standard deviation) or as CV (coefficient of variation = SD/mean diameter) was limited (2.1 mm = 5.0% for the axial diameter; 3.6 mm = 10.0% for the transverse diameter) and smaller than for many currently available electrodes [38,51], which enhances the *predictability of the size* of the ablation.

4.5. FEM modelling

FEM modelling of both the electric field and the temperature distribution was very helpful to improve insight into the 'pathogenesis' of the ablation zones that were obtained in the ex vivo experiments by changing electric mode and activation mode. The simulations enabled us to see the *underlying* invisible phenomena such as electric field and temperature distribution. FEM also allowed to calculate the newly introduced concept of heating efficacy, which was defined as the amount of energy delivered in the target volume (in this study between the active parts of the four electrodes) divided by the total amount of energy delivered. To our best knowledge, this is the first paper to describe and apply software to simulate the *end result* of switching radiofrequency ablation [13].

Simulations of the temperature distribution by FEM modelling closely resembled size and shape of coagulation zones in the ex vivo experiments when using the 60 °C isotherm. Completeness of coagulation however was overestimated by FEM-modelling in 2 out of 6 modes: the monopolar switching and the bipolar switching mode. The reason for this discrepancy is not clear. We suspect that it could be due to the inhomogeneous structure of real liver tissue, in contrast to the artificially homogenous nature of simulated liver tissue. This way, small areas of poor electric conductivity may be responsible for focal areas of overheating and dehydration, focally redirecting (and concentrating) electric flow, disturbing homogeneous electric heating and jeopardising the final coagulation result. Similarly, small areas of poor thermal conductivity may form a barrier for the even spread of thermal energy beyond.

4.6. Matrix radiofrequency ablation (MRFA)

The current experiments in ex vivo liver have shown that a complete coagulation zone of a 3 × 2 × 2 cm block was obtained most efficiently in the bipolar simultaneous mode.

We hope that by adding up these predictable building blocks in MRFA, the entire coagulation zone will be completely coagulated with little coagulation outside. For MRFA, the tumor is pierced by x times y parallel electrodes [51]. The electrodes determine (x-1) times (y-1) rectangular tissue blocks, each boarded by a 2 × 2 electrodes cage. The length of the active parts of each electrode and the distance between two electrodes can be varied within certain limits, as long as the coagulation zone within each 2 × 2 electrodes cage is guaranteed to be complete, so that the sum of all these the blocks closely approaches the size and shape of the tumor including a safety margin around. Coagulation of the whole volume is obtained by activation of the 2 × 2 electrodes around the first block, then rapidly switching to the electrodes around the second block etc. until impedance has risen at all blocks preventing further current flow.

Several steps still need to be taken in the development of MRFA: the current ex vivo studies have to be confirmed in *in vivo* studies; additional experiments are needed to study the results with electrodes that have active tips that are shorter and longer than 3 cm; and the observed reliable coagulation with 2 × 2 electrodes needs to be confirmed when using x times y electrodes. Lastly, the achievements of MRFA using a grid of multiple plain electrodes inside and outside the tumor, encompassing the tumor and a safety margin and activated in a bipolar mode, will have to be compared with the recent technique of no-touch RFA in which multiple bipolar electrodes are placed at the periphery of the tumor without piercing it [56,57,116], with other ablation methods such as microwave [128] and irreversible electroporation [129] (especially regarding efficiency near blood vessels [130]) and with stereotactic body radiotherapy [82].

Of note, if successful, MRFA will need to be performed by laparotomy since parallel placement of electrodes through a percutaneous or laparoscopic approach will be very difficult. Strict parallel placement of the electrodes is mandatory to avoid distortion of the electric field and hence the shape of the ablation zone [131–134]. Mobilisation of the liver may be necessary for locations that are difficult to reach [135]. In theory, ablation could be performed after inserting multiple single electrodes in a pattern that can be composed freely with individual electrodes inserted through holes in a guiding block or a perforated mesh grid, guided by intraoperative ultrasound. This may however be cumbersome and time consuming and parallel placement may be

unsatisfactory [133]. In daily practice, a 'scout' electrode will be inserted into the center of the tumor under ultrasound guidance. A preformatted cluster adapted to the size and shape of the tumor will then be slid over the scout electrode. For spherical tumors, standard clusters will need to be available in different sizes. In case of non spherical tumors, a tailored cluster can be assembled before the procedure based on preoperative imaging. Electrodes should be firmly attached to the body of the cluster to avoid deviation [133] and should be stiff enough to avoid bending, both resulting in non-parallel placement [136].

4.7. The future of RFA: refining FEM modelling or improving reliability of RFA technology?

The initial Pennes' bioheat equation for FEM modelling of RFA is constantly being refined, taking into account more and more electrophysical phenomena such as the heat-sink effect [137], evaporation, water shift and pressure increase [138] and the temperature dependency of electrophysical features [51,139–142]. More accurate simulation has been proposed as a way to improve reliability and safety of clinical ablation in patients [143]. While FEM modelling is no doubt very helpful to assist research and development of radiofrequency ablation electrodes and protocols [138,144], it is not sure whether FEM modelling will ever be able to predict size and shape of ablations in patients with enough accuracy to completely avoid incomplete ablation and collateral damage. The main reason for this caveat is that most FEM models use estimated *mean* values for tissue characteristics *derived from literature* and assume that these characteristics are *homogeneous* throughout the tissue. The composition and therefore the electrical and thermal characteristics of any liver tumor and the surrounding liver parenchyma however are *variable* from one patient to another [42,145–147]. Further, tissue composition is *heterogeneous* on a macroscopic and a microscopic level [148]. Small vessels or small strands of connective tissue may have a non-negligible effect upon the shape of the coagulation zone causing irregular recesses and protrusions [133]. Coagulation of vessels may induce infarction of tissue beyond the area that is coagulated by heat in a way that is difficult to predict. Lastly, real-time exact tissue characteristics of a given tissue are *unknown*, although attempts are being made to measure them before or during the ablation [143,149]. A small change in value of electrical and thermal characteristics can have a large impact in the outcome of the calculated ablation size in a mathematical model [147]. Variability of ablation size obtained with any radiofrequency electrode (system) including ours seems inevitable and is found even in the most standardised ex vivo experiment [38,51].

In view of the above, we feel that refining FEM modelling is certainly helpful but that it will not be sufficient to ensure with certainty complete ablation and to avoid excessive ablation of non tumorous tissue in clinical practice.

We are expecting more progress coming from improving RFA technology itself, which ideally should be able to yield 100% coagulation within a predetermined target volume with minimal coagulation outside, independent of the electrical, thermal and microstructural characteristics of the tissue. We believe that bipolar simultaneous RFA, which has been designed to coagulate all tissue contained within a 2×2 electrodes cage, deserves to be explored further whether it is able to reach this goal or not.

5. Conclusion

In summary, we developed a four electrode system with simple electrodes with a 3 cm active tip and determined its optimal electric and activation mode. In the optimal setting (bipolar simultaneous mode), the coagulation zone was obtained in a short time, very predictable in size and shape and always complete without voids.

FEM modelling was very useful to understand the 'pathogenesis' of RF ablation zones. The good performance of the bipolar simultaneous mode is due to the combination of the higher heating efficiency of the bipolar mode and the lower impedance by the simultaneous activation of four electrodes. The four electrode system used in a bipolar simultaneous mode offers the best perspectives as building block for MRFA. These results obtained in ex vivo liver should be confirmed by in vivo experiments.

Declaration of competing interest

This work was partially supported by the grants awarded by the KU Leuven Molecular Small Animal Imaging Center MoSAIC (KUL EF/05/08); the center of excellence In vivo Molecular Imaging Research (IMIR) of KU Leuven; and a European Union project Asia-Link CfP 2006- Europe Aid/123738/C/ACT/Multi-Proposal No. 128–498/111. Yicheng Ni is currently a Bayer Lecture Chair holder. The authors alone are responsible for the content and writing of the paper.

Acknowledgements

The authors wish to thank Marie-Bernadette Jacqmain and Christian Deneffe for the illustrations. This work was partially supported by MoSAIC, IMIR projects of KU Leuven and EU higher education project Asia-Link CfP 2006-EuropeAid/123738/C/ACT/Multi-Proposal No. 128–498/111.

Appendix A. Supplementary data

Supplementary data to this article can be found online at https://doi.org/10.1016/j.suronc.2020.02.005.

References

[1] A. Casadei Gardini, G. Marisi, M. Canale, F.G. Foschi, G. Donati, G. Ercolani, et al., Radiofrequency ablation of hepatocellular carcinoma: a meta-analysis of overall survival and recurrence-free survival, OncoTargets Ther. 11 (2018) 6555–6567.
[2] T. Ruers, F. Van Coevorden, C.J. Punt, J.E. Pierie, I. Borel-Rinkes, J. A. Ledermann, et al., Local treatment of unresectable colorectal liver metastases: results of a randomized phase II trial, J. Natl. Cancer Inst. 109 (2017).
[3] M. Liao, X. Zhong, J. Zhang, Y. Liu, Z. Zhu, H. Wu, et al., Radiofrequency ablation using a 10-mm target margin for small hepatocellular carcinoma in patients with liver cirrhosis: a prospective randomized trial, J. Surg. Oncol. 115 (2017) 971–979.
[4] S. Ke, X.M. Ding, X.J. Qian, Y.M. Zhou, B.X. Cao, K. Gao, et al., Radiofrequency ablation of hepatocellular carcinoma sized > 3 and ≤ 5 cm: is ablative margin of more than 1 cm justified? World J. Gastroenterol. 19 (2013) 7389–7398.
[5] B.B. Jiang, K. Yan, Z.Y. Zhang, W. Yang, W. Wu, S.S. Yin, et al., The value of KRAS gene status in predicting local tumor progression of colorectal liver metastases following radiofrequency ablation, Int. J. Hyperther. 36 (2019) 211–219.
[6] J.P. McGahan, J.M. Brock, H. Tesluk, W. Gu, P. Schneider, P.D. Browning, Hepatic ablation with use of radio frequency electrocautery in the animal model, J. Vasc. Intervent. Radiol. 3 (1992) 291–297.
[7] S. Mulier, Y. Miao, P. Mulier, B. Dupas, P. Pereira, T. de Baere, et al., Electrodes and multiple electrode systems for radiofrequency ablation: a proposal for updated terminology, Eur. Radiol. 15 (2005) 798–808.
[8] S.A. Solazzo, M. Ahmed, Z. Liu, A.U. Hines-Peralta, S.N. Goldberg, High-power generator for radiofrequency ablation: larger electrodes and pulsing algorithms in bovine ex vivo and porcine in vivo settings, Radiology 242 (2007) 743–750.
[9] S.N. Goldberg, M.C. Stein, G.S. Gazelle, R.G. Sheiman, J.B. Kruskal, M.E. Clouse, Percutaneous radiofrequency tissue ablation: optimization of pulsed radiofrequency technique to increase coagulation necrosis, J. Vasc. Intervent. Radiol. 10 (1999) 907–916.
[10] M. Kobayashi, K. Ikeda, T. Someya, N. Akuta, F. Suzuki, A. Tsubota, et al., Stepwise hook extension technique for radiofrequency ablation therapy of hepatocellular carcinoma, Oncology 63 (2002) 139–144.
[11] J.P. McGahan, S. Loh, F.J. Boschini, E.E. Paoli, J.M. Brock, W.L. Monsky, et al., Maximizing parameters for tissue ablation by using an internally cooled electrode, Radiology 256 (2010) 397–405.
[12] M. Koda, S. Tokunaga, T. Matono, T. Sugihara, T. Nagahara, Y. Murawaki, Comparison between different thickness umbrella-shaped expandable radiofrequency electrodes (SuperSlim and CoAccess): experimental and clinical study, Exp. Ther. Med. 2 (2011) 1215–1220.
[13] D. Haemmerich, F.T. Lee Jr., D.J. Schutt, L.A. Sampson, J.G. Webster, J.P. Fine, et al., Large-volume radiofrequency ablation of ex vivo bovine liver with multiple cooled cluster electrodes, Radiology 234 (2005) 563–568.
[14] A.L. Denys, T. De Baere, V. Kuoch, B. Dupas, P. Chevallier, D.C. Madoff, et al., Radio-frequency tissue ablation of the liver: in vivo and ex vivo experiments with four different systems, Eur. Radiol. 13 (2003) 2346–2352.

[15] S. Mulier, Y. Ni, Y. Miao, A. Rosière, A. Khoury, G. Marchal, et al., Size and geometry of hepatic radiofrequency lesions, Eur. J. Surg. Oncol. 29 (2003) 867–878.
[16] E. Berber, N.L. Herceg, K.J. Casto, A.E. Siperstein, Laparoscopic radiofrequency ablation of hepatic tumors: prospective clinical evaluation of ablation size comparing two treatment algorithms, Surg. Endosc. 18 (2004) 390–396.
[17] R.S. Montgomery, A. Rahal, G.D. Dodd 3rd, J.R. Leyendecker, L.G. Hubbard, Radiofrequency ablation of hepatic tumors: variability of lesion size using a single ablation device, AJR Am. J. Roentgenol. 182 (2004) 657–661.
[18] P.L. Pereira, J. Trubenbach, M. Schenk, J. Subke, S. Kroeber, I. Schaefer, et al., Radiofrequency ablation: in vivo comparison of four commercially available devices in pig livers, Radiology 232 (2004) 482–490.
[19] D.L. Stippel, H.G. Brochhagen, M. Arenja, J. Hunkemoller, A.H. Holscher, K. T. Beckurts, Variability of size and shape of necrosis induced by radiofrequency ablation in human livers: a volumetric evaluation, Ann. Surg Oncol. 11 (2004) 420–425.
[20] B.B. Frericks, J.P. Ritz, A. Roggan, K.J. Wolf, T. Albrecht, Multipolar radiofrequency ablation of hepatic tumors: initial experience, Radiology 237 (2005) 1056–1062.
[21] S. Mulier, Y. Ni, J. Jamart, T. Ruers, G. Marchal, L. Michel, Local recurrence after hepatic radiofrequency coagulation: multivariate meta-analysis and review of contributing factors, Ann. Surg. 242 (2005) 158–171.
[22] L. Frich, T. Mala, I.P. Gladhaug, Hepatic radiofrequency ablation using perfusion electrodes in a pig model: effect of the Pringle manoeuvre, Eur. J. Surg. Oncol. 32 (2006) 527–532.
[23] A. Oshio, K. Tamaki, I. Shimizu, H. Fukuno, M. Urata, S. Ito, et al., Double radiofrequency ablation is more extensive with a spherical zone shape compared to single ablation in a pig liver model, J. Med. Invest. 54 (2007) 28–34.
[24] Boykin Rex Douglas, Characterization of Radiofrequency Ablation Zonesfor the Purpose of Treatment Planning. A Dissertation Presented to the Faculty of the University of Texas Health Science Center at San Antonio Graduate School of Biomedical Sciences in Partial Fulfillment of the Requirements for the Degree of Doctor of Philosophy, San Antonio, Texas, December, 2008.
[25] M. Hirakawa, K. Ikeda, Y. Kawamura, M. Kobayashi, T. Hosaka, H. Yatsuji, et al., New ablation procedure for a radiofrequency liver tissue coagulation system using an expandable needle, Liver Int. 28 (2008), 214-209.
[26] N. Bhardwaj, A.D. Strickland, F. Ahmad, L. Atanesyan, K. West, D.M. Lloyd, A comparative histological evaluation of the ablations produced by microwave, cryotherapy and radiofrequency in the liver, Pathology 41 (2009) 168–172.
[27] J. Cha, D. Choi, M.W. Lee, H. Rhim, Y.S. Kim, H.K. Lim, et al., Radiofrequency ablation zones in ex vivo bovine and in vivo porcine livers: comparison of the use of internally cooled electrodes and internally cooled wet electrodes, Cardiovasc. Intervent. Radiol. 32 (2009) 1235–1240.
[28] D. Schmidt, S. Clasen, A. Boss, T. Herberts, C. Aubé, J. Truebenbach, et al., Comparison of a single perfusion device and an internally cooled cluster device: laboratory experience in ex vivo liver tissue with longer duration of energy application, J. Vasc. Intervent. Radiol. 20 (2009) 524–531.
[29] D.L. Stippel, C. Bangard, K. Prenzel, S. Yavuzyasar, J.H. Fischer, A.H. Hölscher, Which parameters are needed for targeting a multitined radiofrequency device-an approach to a simple algorithm, Langenbeck's Arch. Surg. 394 (2009) 671–679.
[30] R. Wahba, C. Bangard, R. Kleinert, S. Rösgen, J.H. Fischer, K.J. Lackner, et al., Electro-physiological parameters of hepatic radiofrequency ablation-a comparison of an in vitro versus an in vivo porcine liver model, Langenbeck's Arch. Surg. 394 (2009) 503–509.
[31] C. Bangard, S. Rösgen, R. Wahba, R. Wiemker, M. Hellmich, H. Reiter, et al., Large-volume multi-tined expandable RF ablation in pig livers: comparison of 2D and volumetric measurements of the ablation zone, Eur. Radiol. 20 (2010) 1073–1078.
[32] C. Kawamoto, A. Yamauchi, Y. Baba, K. Kaneko, K. Yakabi, Measurement of intrahepatic pressure during radiofrequency ablation in porcine liver, J. Gastroenterol. 45 (2010) 435–442.
[33] A. Orlacchio, A. Mancini, G. Calabrese, F. Bolacchi, V. Cozzolino, M. Angelico, et al., Portal vein thrombosis after radiofrequency ablation of HCC, Minerva Gastroenterol. Dietol. 56 (2010) 87–91.
[34] F. Burdio, P. Tobajas, R. Quesada-Diez, E. Berjano, A. Navarro, I. Poves, et al., Distant infusion of saline may enlarge coagulation volume during radiofrequency ablation of liver tissue using cool-tip electrodes without impairing predictability, AJR Am. J. Roentgenol. 196 (2011) W837–W843.
[35] M. Seise, T. Alhonnoro, M. Kolesnik, Interactive registration of 2D histology and 3D CT data for assessment of radiofrequency ablation treatment, J. Pathol. Inf. 2 (2011) S9.
[36] G.D. Dodd 3rd, N.A. Dodd, A.C. Lanctot, D.A. Glueck, Effect of variation of portal venous blood flow on radiofrequency and microwave ablations in a blood-perfused bovine liver model, Radiology 267 (2013) 129–136.
[37] M. Hirakawa, K. Ikeda, M. Kobayashi, Y. Kawamura, T. Hosaka, H. Sezaki, et al., Randomized controlled trial of a new procedure of radiofrequency ablation using an expandable needle for hepatocellular carcinoma, Hepatol. Res. 43 (2013) 846–852.
[38] H. Rathke, B. Hamm, F. Güttler, J. Rathke, J. Rump, U. Teichgräber, et al., Comparison of four radiofrequency ablation systems at target volumes of 3 and 5 cm in an ex vivo bovine liver model, Diagn. Interv. Radiol. 20 (2014) 251–258.
[39] H. Rempp, D. Mezger, M. Voigtlaender, M. Scharpf, R. Hoffmann, P.L. Pereira, et al., A comparison of internally water-perfused and cryogenically cooled monopolar and bipolar radiofrequency applicators in ex vivo liver samples, Acad. Radiol. 21 (2014) 661–666.
[40] H. Tang, Y. Tang, J. Hong, T. Chen, C. Mai, P. Jiang, A measure to assess the ablative margin using 3D-CT image fusion after radiofrequency ablation of hepatocellular carcinoma, HPB (Oxford) 17 (2015) 318–325.
[41] J.H. Yoon, J.M. Lee, S. Woo, E.J. Hwang, I. Hwang, W. Choi, et al., Switching bipolar hepatic radiofrequency ablation using internally cooled wet electrodes: comparison with consecutive monopolar and switching monopolar modes, Br. J. Radiol. 88 (2015), 20140468.
[42] B. Duan, R. Wen, Y. Fu, K.J. Chua, C.K. Chui, Probabilistic finite element method for large tumor radiofrequency ablation simulation and planning, Med. Eng. Phys. 38 (2016) 1360–1368.
[43] F.G. Poch, C. Rieder, H. Ballhausen, V. Knappe, J.P. Ritz, O. Gemeinhardt, et al., The vascular cooling effect in hepatic multipolar radiofrequency ablation leads to incomplete ablation ex vivo, Int. J. Hyperther. 32 (2016) 749–756.
[44] T. Tanaka, K. Ikeda, Y. Sorin, T. Fukushima, Y. Kawamura, M. Kobayashi, et al., Three-dimensional imaging using contrast-enhanced and three-dimensional ultrasound techniques in the ablative zone treated with a multipolar radiofrequency ablation system for hepatocellular carcinoma, Oncology 90 (2016) 255–260.
[45] S. Chang, A.C. Lanctot, M.D. McCarter, K.M. Roberts, D.H. Glueck, G.D. Dodd 3rd, The prediction of radiofrequency ablation zone volume using vascular indices of 3-dimensional volumetric colour Doppler ultrasound in an in vitro blood-perfused bovine liver model, Br. J. Radiol. 90 (2017) 20160661.
[46] W. Chang, J.M. Lee, J.H. Yoon, D.H. Lee, S.M. Lee, K.B. Lee, et al., No-touch radiofrequency ablation using multiple electrodes: an in vivo comparison study of switching monopolar versus switching bipolar modes in porcine livers, PloS One 12 (2017), e0176350.
[47] P. Mariappan, P. Weir, R. Flanagan, P. Voglreiter, T. Alhonnoro, M. Pollari, et al., GPU-based RFA simulation for minimally invasive cancer treatment of liver tumours, Int. J. Comput. Assist. Radiol. Surg. 12 (2017) 59–68.
[48] J.L. Vahldiek, C. Erxleben, K.K. Bressem, O. Gemeinhardt, F. Poch, B. Hiebl, et al., Multipolar RFA of the liver: influence of intrahepatic vessels on ablation zones and appropriateness of CECT in detecting ablation dimensions - results of an in-vivo porcine liver model, Clin. Hemorheol. Microcirc. 70 (2018) 467–476.
[49] P. Voglreiter, P. Mariappan, M. Pollari, R. Flanagan, R. Blanco Sequeiros, R. H. Portugaller, et al., RFA Guardian: comprehensive simulation of radiofrequency ablation treatment of liver tumors, Sci. Rep. 8 (2018) 787.
[50] R. Yoshimatsu, A. Doi, T. Yamanishi, M. Nishimori, K. Ogi, K. Kajiwara, et al., Prediction of the ablated area prior to radiofrequency ablation for liver tumor under CT guidance, Minim Invasive Ther. Allied Technol. 27 (2018) 22–26.
[51] S. Mulier, Y. Jiang, J. Jamart, C. Wang, Y. Feng, G. Marchal, et al., Bipolar radiofrequency ablation with 2 × 2 electrodes as a building block for matrix radiofrequency ablation: ex vivo liver experiments and finite element method modelling, Int. J. Hyperther. 31 (2015) 649–665.
[52] J. Ding, X. Jing, J. Liu, Y. Wang, F. Wang, Y. Wang, et al., Comparison of two different thermal techniques for the treatment of hepatocellular carcinoma, Eur. J. Radiol. 82 (2013) 1379–1384.
[53] C. Wang, H. Wang, W. Yang, K. Hu, H. Xie, K.Q. Hu, et al., Multicenter randomized controlled trial of percutaneous cryoablation versus radiofrequency ablation in hepatocellular carcinoma, Hepatology 61 (2015) 1579–1590.
[54] X. Xie, C. Jiang, Z. Peng, B. Liu, W. Hu, Y. Wang, et al., Local recurrence after radiofrequency ablation of hepatocellular carcinoma: treatment choice and outcome, J. Gastrointest. Surg. 19 (2015) 1466–1475.
[55] F. Shi, Z. Tan, H. An, X. Wang, Y. Xu, S. Wang, Hepatocellular carcinoma ≤ 4 cm treated with radiofrequency ablation with or without percutaneous ethanol injection, Ann. Hepatol. 15 (2016) 61–70.
[56] A. Hocquelet, C. Aubé, A. Rode, V. Cartier, O. Sutter, A.F. Manichon, et al., Comparison of no-touch multi-bipolar vs. monopolar radiofrequency ablation for small HCC, J. Hepatol. 66 (2017) 67–74.
[57] Y. Kawamura, K. Ikeda, S. Fujiyama, T. Hosaka, M. Kobayashi, S. Saitoh, et al., Potential of a no-touch pincer ablation procedure that uses a multipolar radiofrequency ablation system to prevent intrasubsegmental recurrence of small and single hepatocellular carcinomas, Hepatol. Res. 47 (2017) 1008–1020.
[58] W. Chang, J.M. Lee, D.H. Lee, J.H. Yoon, Y.J. Kim, J.H. Yoon, et al., Comparison of switching bipolar ablation with multiple cooled wet electrodes and switching monopolar ablation with separable clustered electrode in treatment of small hepatocellular carcinoma: a randomized controlled trial, PloS One 13 (2018), e0192173.
[59] Y. Kawamura, K. Ikeda, J. Shindoh, Y. Kobayashi, K. Kasuya, S. Fujiyama, et al., No-touch ablation in hepatocellular carcinoma has the potential to prevent intrasubsegmental recurrence to the same degree as surgical resection, Hepatol. Res. 49 (2019) 164–176.
[60] A. Hocquelet, P. Balageas, C. Laurent, J.F. Blanc, N. Frulio, C. Salut, et al., Radiofrequency ablation versus surgical resection for hepatocellular carcinoma within the Milan criteria: a study of 281 Western patients, Int. J. Hyperther. 31 (2015) 749–757.
[61] S.J. Lee, E.H. Cho, R. Kim, Y.H. Kim, C.S. Lim, S.B. Kim, Hepatectomy, combined with intraoperative radiofrequency ablation in patients with multiple hepatocellular carcinomas, Kor. J. Hepatobiliary Pancreat. Surg. 19 (2015) 98–102.
[62] N. Harada, K. Shirabe, T. Maeda, H. Kayashima, S. Takaki, Y. Maehara, Comparison of the outcomes of patients with hepatocellular carcinoma and portal hypertension after liver resection versus radiofrequency ablation, World J. Surg. 40 (2016) 1709–1719.
[63] G.A. Kim, J.H. Shim, M.J. Kim, S.Y. Kim, H.J. Won, Y.M. Shin, et al., Radiofrequency ablation as an alternative to hepatic resection for single small hepatocellular carcinomas, Br. J. Surg. 103 (2016) 126–135.

[64] T.A. Potretzke, T.J. Ziemlewicz, J.L. Hinshaw, M.G. Lubner, S.A. Wells, C. L. Brace, et al., Microwave versus radiofrequency ablation treatment for hepatocellular carcinoma: a comparison of efficacy at a single center, J. Vasc. Intervent. Radiol. 27 (2016) 631–638.
[65] G.C. Vitali, A. Laurent, S. Terraz, P. Majno, N.C. Buchs, L. Rubbia-Brandt, et al., Minimally invasive surgery versus percutaneous radio frequency ablation for the treatment of single small (≤3 cm) hepatocellular carcinoma: a case-control study, Surg. Endosc. 30 (2016) 2301–2307.
[66] S.M. Kim, S.S. Shin, B.C. Lee, J.W. Kim, S.H. Heo, H.S. Lim, et al., Imaging evaluation of ablative margin and index tumor immediately after radiofrequency ablation for hepatocellular carcinoma: comparison between multidetector-row CT and MR imaging, Abdom. Radiol. (NY) 42 (2017) 2527–2537.
[67] H. Nitta, S. Nakagawa, T. Kaida, K. Arima, T. Higashi, K. Taki, et al., Pre-treatment double- or triple-positive tumor markers are predictive of a poor outcome for patients undergoing radiofrequency ablation for hepatocellular carcinoma, Surg. Today 47 (2017) 375–384.
[68] W. Liu, Y. Zheng, W. He, R. Zou, J. Qiu, J. Shen, et al., Microwave vs radiofrequency ablation for hepatocellular carcinoma within the Milan criteria: a propensity score analysis, Aliment. Pharmacol. Ther. 48 (2018) 671–681.
[69] R. Santambrogio, M. Barabino, S. Bruno, N. Mariani, N. Maroni, E. Bertolini, et al., Surgical resection vs. ablative therapies through a laparoscopic approach for hepatocellular carcinoma: a comparative study, J. Gastrointest. Surg. 22 (2018) 650–660.
[70] Y. Takuma, I. Shota, H. Miyatake, S. Uematsu, R. Okamoto, Y. Araki, et al., Nomograms to predict the disease-free survival and overall survival after radiofrequency ablation for hepatocellular carcinoma, Intern. Med. 57 (2018) 457–468.
[71] G. Francica, A. Saviano, I. De Sio, N. De Matthaeis, F. Brunello, A. Cantamessa, et al., Long-term effectiveness of radiofrequency ablation for solitary small hepatocellular carcinoma: a retrospective analysis of 363 patients, Dig. Liver Dis. 45 (2013) 336–341.
[72] M. Pompili, A. Saviano, N. de Matthaeis, A. Cucchetti, F. Ardito, B. Federico, et al., Long-term effectiveness of resection and radiofrequency ablation for single hepatocellular carcinoma ≤3 cm. Results of a multicenter Italian survey, J. Hepatol. 59 (2013) 89–97.
[73] J.Y. Cho, M.S. Choi, G.S. Lee, W. Sohn, J. Ahn, D.H. Sinn, et al., Clinical significance and predictive factors of early massive recurrence after radiofrequency ablation in patients with a single small hepatocellular carcinoma, Clin. Mol. Hepatol. 22 (2016) 477–486.
[74] T. Ito, S. Tanaka, S. Iwai, S. Takemura, A. Hagihara, S. Uchida-Kobayashi, et al., Outcomes of laparoscopic hepatic resection versus percutaneous radiofrequency ablation for hepatocellular carcinoma located at the liver surface: a case-control study with propensity score matching, Hepatol. Res. 46 (2016) 565–574.
[75] Y. Hao, K. Numata, T. Ishii, H. Fukuda, S. Maeda, M. Nakano, et al., Rate of local tumor progression following radiofrequency ablation of pathologically early hepatocellular carcinoma, World J. Gastroenterol. 23 (2017) 3111–3121.
[76] T. Ishii, K. Numata, Y. Hao, N. Doba, K. Hara, M. Kondo, et al., Evaluation of hepatocellular carcinoma tumor vascularity using contrast-enhanced ultrasonography as a predictor for local recurrence following radiofrequency ablation, Eur. J. Radiol. 89 (2017) 234–241.
[77] M.W. Lee, S.S. Raman, N.H. Asvadi, S. Siripongsakun, R.M. Hicks, J. Chen, et al., Radiofrequency ablation of hepatocellular carcinoma as bridge therapy to liver transplantation: a 10-year intention-to-treat analysis, Hepatology 65 (2017) 1979–1990.
[78] R. Santambrogio, J. Chiang, M. Barabino, F.M. Meloni, E. Bertolini, F. Melchiorre, et al., Comparison of laparoscopic microwave to radiofrequency ablation of small hepatocellular carcinoma (≤3 cm), Ann. Surg Oncol. 24 (2017) 257–263.
[79] T. Tamai, A. Oshige, K. Tabu, E. Tabu, S. Ijyuin, H. Sakae, et al., Utility of percutaneous radiofrequency ablation alone or combined with transarterial chemoembolization for early hepatocellular carcinoma, Oncol. Lett. 14 (2017) 3199–3206.
[80] Y. Kato, Y. Okamura, K. Omae, T. Sugiura, T. Ito, Y. Yamamoto, et al., Propensity score-matched comparison of non-anatomical resection and radiofrequency ablation for hepatocellular carcinoma in patients with up to three tumours, each measuring up to 3 cm in diameter, BJS Open 2 (2018) 213–219.
[81] N. Takeyama, N. Mizobuchi, M. Sakaki, Y. Shimozuma, J. Munechika, A. Kajiwara, et al., Evaluation of hepatocellular carcinoma ablative margins using fused pre- and post-ablation hepatobiliary phase images, Abdom. Radiol. (NY) 44 (2019) 923–935.
[82] K. Hara, A. Takeda, Y. Tsurugai, Y. Saigusa, N. Sanuki, T. Eriguchi, et al., Radiotherapy for hepatocellular carcinoma results in comparable survival to radiofrequency ablation: a propensity score analysis [Epub ahead of print], Hepatology 69 (6) (2019 Feb 25) 2533–2545.
[83] A.N. Martin, L.R. Wilkins, D. Das, L.E. Johnston, T.W. Bauer, R.B. Adams, et al., Efficacy of radiofrequency ablation versus transarterial chemoembolization for patients with solitary hepatocellular carcinoma ≤3 cm, Am. Surg. 85 (2019) 150–155.
[84] K.D. Song, H.K. Lim, H. Rhim, M.W. Lee, T.W. Kang, Y.H. Paik, et al., Hepatic resection vs percutaneous radiofrequency ablation of hepatocellular carcinoma abutting right diaphragm, World J. Gastrointest. Oncol. 11 (2019) 227–237.
[85] H. Ding, M. Su, C. Zhu, L. Wang, Q. Zheng, Y. Wan, CT-guided versus laparoscopic radiofrequency ablation in recurrent small hepatocellular carcinoma against the diaphragmatic dome, Sci. Rep. 7 (2017), 44583.
[86] C.C. Chong, K.F. Lee, C.M. Chu, A.W. Chan, S.C. Yu, P.B. Lai, Laparoscopic hepatectomy (with or without robotic assistance) versus radiofrequency ablation as a minimally invasive treatment for very early-stage or early-stage hepatocellular carcinoma, Dig. Surg. (2019 Mar 27) 1–7 [Epub ahead of print].
[87] C.C. Lin, Y.T. Cheng, M.W.T. Chen, S.M. Lin, The effectiveness of multiple electrode radiofrequency ablation in patients with hepatocellular carcinoma with lesions more than 3 cm in size and Barcelona Clinic Liver Cancer stage A to B2, Liver Canc. 5 (2016) 8–20.
[88] T.Q. Zhang, Y.Y. Zhang, Y.K. Gu, F. Gao, Z.M. Huang, J.H. Huang, [Clinical application of multi-electrode synchronous radiofrequency ablation via switching controller for treating large hepatocellular carcinoma], Zhonghua Yixue Zazhi 96 (2016) 2777–2780.
[89] T.J. Kennedy, M.A. Cassera, Y.S. Khajanchee, T.S. Diwan, C.W. Hammill, P. D. Hansen, Laparoscopic radiofrequency ablation for the management of colorectal liver metastases: 10-year experience, J. Surg. Oncol. 107 (2013) 324–328.
[90] K. Nielsen, A.A. van Tilborg, M.R. Meijerink, M.O. Macintosh, B.M. Zonderhuis, E. S. de Lange, et al., Incidence and treatment of local site recurrences following RFA of colorectal liver metastases, World J. Surg. 37 (2013) 1340–1347.
[91] E. Tanis, B. Nordlinger, M. Mauer, H. Sorbye, F. van Coevorden, T. Gruenberger, et al., Local recurrence rates after radiofrequency ablation or resection of colorectal liver metastases. Analysis of the European Organisation for Research and Treatment of Cancer #40004 and #40983, Eur. J. Canc. 50 (2014) 912–919.
[92] C. Valls, E. Ramos, D. Leiva, S. Ruiz, L. Martinez, A. Rafecas, Safety and efficacy of ultrasound-guided radiofrequency ablation of recurrent colorectal cancer liver metastases after hepatectomy, Scand. J. Surg. 104 (2015) 169–175.
[93] K. Imai, M.A. Allard, C. Castro Benitez, E. Vibert, A. Sa Cunha, D. Cherqui, et al., Long-term outcomes of radiofrequency ablation combined with hepatectomy compared with hepatectomy alone for colorectal liver metastases, Br. J. Surg. 104 (2017) 570–579.
[94] H. Takahashi, M. Akyuz, B. Kahramangil, E. Kose, F. Aucejo, J. Fung, et al., A comparison of the initial cost associated with resection versus laparoscopic radiofrequency ablation of small solitary colorectal liver metastasis, Surg. Laparosc. Endosc. Percutaneous Tech. 28 (2018) 371–374.
[95] N. Vietti Violi, R. Duran, N. Demartines, C. Sempoux, B. Guiu, P.E. Bize, et al., Local recurrence rate in patients with colorectal cancer liver metastasis after wedge resection or percutaneous radiofrequency ablation, Int. J. Hyperther. 34 (2018) 1020–1028.
[96] S. Aliyev, O. Agcaoglu, E. Aksoy, H.E. Taskin, D. Vogt, J. Fung, et al., Efficacy of laparoscopic radiofrequency ablation for the treatment of patients with small solitary colorectal liver metastasis, Surgery 154 (2013) 556–562.
[97] B.C. Lee, H.G. Lee, I.J. Park, S.Y. Kim, K.H. Kim, J.H. Lee, et al., The role of radiofrequency ablation for treatment of metachronous isolated hepatic metastasis from colorectal cancer, Medicine (Baltim.) 95 (2016), e4999.
[98] A.A. van Tilborg, H.J. Scheffer, M.C. de Jong, L.G. Vroomen, K. Nielsen, C. van Kuijk, et al., MWA versus RFA for perivascular and peribiliary CRLM: a retrospective patient- and lesion-based analysis of two historical cohorts, Cardiovasc. Intervent. Radiol. 39 (2016) 1438–1446.
[99] X. Wang, C.T. Sofocleous, J.P. Erinjeri, E.N. Petre, M. Gonen, K.G. Do, et al., Margin size is an independent predictor of local tumor progression after ablation of colon cancer liver metastases, Cardiovasc. Intervent. Radiol. 36 (2013) 166–175.
[100] S. Iwamura, T. Iida, H. Terajima, H. Matsubara, T. Goto, Y. Inoue, et al., Hepatic resection for local recurrence after radiofrequency ablation therapy for colorectal liver metastases, Gan To Kagaku Ryoho 41 (2014) 2062–2064.
[101] W. Shady, E.N. Petre, M. Gonen, J.P. Erinjeri, K.T. Brown, A.M. Covey, et al., Percutaneous radiofrequency ablation of colorectal cancer liver metastases: factors affecting outcomes–A 10-year experience at a single center, Radiology 278 (2016) 601–611.
[102] W. Shady, E.N. Petre, E. Vakiani, E. Ziv, M. Gonen, K.T. Brown, et al., Kras mutation is a marker of worse oncologic outcomes after percutaneous radiofrequency ablation of colorectal liver metastases, Oncotarget 8 (2017) 66117–66127.
[103] N. Zhang, H. Li, C. Qin, D. Ma, Y. Zhao, W. Zhu, et al., Insufficient radiofrequency ablation promotes the metastasis of residual hepatocellular carcinoma cells via upregulating flotillin proteins, J. Canc. Res. Clin. Oncol. 145 (2019) 895–907.
[104] M.W. Nijkamp, F.J. Hoogwater, E.J. Steller, B.F. Westendorp, T.A. van der Meulen, M.W. Leenders, et al., CD95 is a key mediator of invasion and accelerated outgrowth of mouse colorectal liver metastases following radiofrequency ablation, J. Hepatol. 53 (2010) 1069–1077.
[105] S. Yamagishi, Y. Midorikawa, H. Nakayama, T. Higaki, M. Moriguchi, O. Aramaki, et al., Liver resection for recurrent hepatocellular carcinoma after radiofrequency ablation therapy, Hepatol. Res. 49 (2019) 432–440.
[106] S. Ou, R. Xu, K. Li, Y. Chen, Y. Kong, H. Liu, et al., Radiofrequency ablation with systemic chemotherapy in the treatment of colorectal cancer liver metastasis: a 10-year single-center study, Canc. Manag. Res. 10 (2018) 5227–5237.
[107] L. Viganò, A. Laurenzi, L. Solbiati, F. Procopio, D. Cherqui, G. Torzilli, Open liver resection, laparoscopic liver resection, and percutaneous thermal ablation for patients with solitary small hepatocellular carcinoma (≤30 mm): review of the literature and proposal for a therapeutic strategy, Dig. Surg. 35 (2018) 359–371.
[108] K.H. Kim, Y.S. Yoon, C.S. Yu, T.W. Kim, H.J. Kim, P.N. Kim, et al., Comparative analysis of radiofrequency ablation and surgical resection for colorectal liver metastases, J. Korean Surg. Soc. 81 (2011) 25–34.
[109] M.R. Meijerink, R.S. Puijk, A.A.J.M. van Tilborg, K.H. Henningsen, L. G. Fernandez, M. Neyt, et al., Radiofrequency and microwave ablation compared to systemic chemotherapy and to partial hepatectomy in the treatment of colorectal liver metastases: a systematic review and meta-analysis, Cardiovasc. Intervent. Radiol. 41 (2018) 1189–1204.

[110] S.R. Venkat, P.P. Mohan, R.T. Gandhi, Colorectal Liver Metastasis: overview of treatment paradigm highlighting the role of ablation, AJR Am. J. Roentgenol. 210 (2018) 883–890.
[111] B. Zhang, M.A. Moser, E.M. Zhang, Y. Luo, C. Liu, W. Zhang, A review of radiofrequency ablation: large target tissue necrosis and mathematical modelling, Phys. Med. 32 (2016) 961–971.
[112] S. Thamtorawat, R.M. Hicks, J. Yu, S. Siripongsakun, W.C. Lin, S.S. Raman, et al., Preliminary outcome of microwave ablation of hepatocellular carcinoma: breaking the 3-cm barrier? J. Vasc. Intervent. Radiol. 27 (2016) 623–630.
[113] K.R. Kim, S. Thomas, Complications of image-guided thermal ablation of liver and kidney neoplasms, Semin. Intervent. Radiol. 31 (2014) 138–148.
[114] E. Lahat, R. Eshkenazy, A. Zendel, B.B. Zakai, M. Maor, Y. Dreznik, et al., Complications after percutaneous ablation of liver tumors: a systematic review, Hepatobiliary Surg. Nutr. 3 (2014) 317–323.
[115] L.W. Wu, C.Y. Chen, C.L. Liu, M.Y. Chen, P.C. Liu, P.F. Liu, et al., Multipolar radiofrequency ablation with non-touch technique for hepatocellular carcinoma $\leq$ 3 cm: a preliminary report, Adv. Digest. Med. 1 (2014) 80–85.
[116] O. Seror, G. N'Kontchou, J.C. Nault, Y. Rabahi, P. Nahon, N. Ganne-Carrié, et al., Hepatocellular carcinoma within Milan criteria: no-touch multi bipolar radiofrequency ablation for treatment-long-term results, Radiology 280 (2016) 981.
[117] S. Mulier, Y. Jiang, C. Wang, J. Jamart, G. Marchal, L. Michel, et al., Bipolar radiofrequency ablation with four electrodes: ex vivo liver experiments au niveau de finite element method analysis. Influence of inter-electrode distance on coagulation size and geometry, Int. J. Hyperther. 28 (2012) 686–697.
[118] F.T. Lee, D. Haemmerich, A.W. Wright, D.M. Mahvi, L.A. Sampson, J.G. Webster, Multiple probe radiofrequency ablation : pilot study in an animal model, J. Vasc. Intervent. Radiol. 14 (2003) 1437–1442.
[119] D. Haemmerich, S.T. Staelin, S. Tungjitkusolmun, F.T. Lee Jr., D.M. Mahvi, J. G. Webster, Hepatic bipolar radio-frequency ablation between separated multiprong electrodes, IEEE Trans. Biomed. Eng. 48 (2001) 1145–1152.
[120] I. Al-Alem, K. Pillai, J. Akhter, T.C. Chua, D.L. Morris, Heat sink phenomenon of bipolar and monopolar radiofrequency ablation observed using polypropylene tubes for vessel simulation, Surg. Innovat. 21 (2014) 269–276.
[121] K. Pillai, J. Akhter, T.C. Chua, M. Shehata, N. Alzahrani, I. Al-Alem, et al., Heat sink effect on tumor ablation characteristics as observed in monopolar radiofrequency, bipolar radiofrequency, and microwave, using ex vivo calf liver model, Medicine (Baltim.) 94 (2015), e580.
[122] K.S. Lehmann, F.G. Poch, C. Rieder, A. Schenk, A. Stroux, B.B. Frericks, et al., Minimal vascular flows cause strong heat sink effects in hepatic radiofrequency ablation ex vivo, J. Hepatobiliary Pancreat. Sci. 23 (2016) 508–516.
[123] G.D. Dodd 3rd, A.C. Lanctot, K.E. Lind, Effect of change in portal vein flow rates on hepatic ablations created with a bipolar radiofrequency ablation device, Radiology 283 (2017) 399–407.
[124] D. Haemmerich, S. Tungjitkusolmun, S.T. Staelin, F.T. Lee Jr., D.M. Mahvi, J. G. Webster, Finite-element analysis of hepatic multiple probe radio-frequency ablation, IEEE Trans. Biomed. Eng. 49 (2002) 836–842.
[125] J.M. Lee, H. Rhim, J.K. Han, B.J. Youn, S.H. Kim, B.I. Choi, Dual-probe radiofrequency ablation: an in vitro experimental study in bovine liver, Invest. Radiol. 39 (2004) 89–96.
[126] M. Frieser, S. Schaber, A. Peters, T. Bernatik, T. Haendl, E.G. Hahn, et al., Radiofrequency ablation using perfused needle electrodes - study of intermittent and continuous triple needle application ex vivo, Eur. Surg. Res. 37 (2005) 312–316.
[127] J.M. Lee, J.K. Han, S.H. Kim, C.J. Han, S.K. An, J.Y. Lee, et al., Wet radio-frequency ablation using multiple electrodes: comparative study of bipolar versus monopolar modes in the bovine liver, Eur. J. Radiol. 54 (2005) 408–417.
[128] S.J.S. Ruiter, W.J. Heerink, K.P. de Jong, Liver microwave ablation: a systematic review of various FDA-approved systems, Eur. Radiol. 28 (2018) 3228–3236.
[129] A. Saini, I. Breen, S. Alzubaidi, Y. Pershad, R. Sheth, S. Naidu, et al., Irreversible electroporation in liver cancers and whole organ engineering, J. Clin. Med. 8 (2018) pii: E22.
[130] A.S. Wright, L.A. Sampson, T.F. Warner, D.M. Mahvi, F.T. Lee Jr., Radiofrequency versus microwave ablation in a hepatic porcine model, Radiology 236 (2005) 132–139.
[131] B. Yi, P. Somasundar, N.J. Espat, Novel laparoscopic bipolar radiofrequency energy technology for expedited hepatic tumour ablation, HPB (Oxford) 11 (2009) 135–139.
[132] E.R. Cosman Jr., C.D. Gonzalez, Bipolar radiofrequency lesion geometry: implications for palisade treatment of sacroiliac joint pain, Pain Pract. 11 (2011) 3–22.
[133] R. Stoffner, C. Kremser, P. Schullian, M. Haidu, G. Widmann, R.J. Bale, Multipolar radiofrequency ablation using 4-6 applicators simultaneously: a study in the ex vivo bovine liver, Eur. J. Radiol. 81 (2012) 2568–2575.
[134] K. Pillai, I. Al-Alem, J. Akhter, T.C. Chua, M. Shehata, D.L. Morris, Effect of nonparallel placement of in-circle bipolar radiofrequency ablation probes on volume of tissue ablated with heat sink, Surg. Innovat. 22 (2015) 223–234.
[135] K. Baldwin, S.C. Katz, A. Rubin, P. Somasundar, Bipolar radiofrequency ablation of liver tumors: technical experience and interval follow-up in 22 patients with 33 ablations, J. Surg. Oncol. 106 (2012) 905–910.
[136] H.J. Park, M.W. Lee, K.D. Song, D.I. Cha, H. Rhim, T.W. Kang, et al., Comparison of therapeutic efficacy and safety of radiofrequency ablation of hepatocellular carcinomas between internally cooled 15-G and 17-G single electrodes, Br. J. Radiol. 87 (2014), 20130534.
[137] R. Chen, F. Lu, F. Wu, T. Jiang, L. Xie, D. Kong, An analytical solution for temperature distributions in hepatic radiofrequency ablation incorporating the heat-sink effect of large vessels, Phys. Med. Biol. 63 (2018), 235026.
[138] W. Karaki, Rahul, C.A. Lopez, D.A. Borca-Tasciuc, S. De, A continuum thermomechanical model of in vivo electrosurgical heating of hydrated soft biological tissues, Int. J. Heat Mass Tran. 127 (Pt A) (2018) 961–974.
[139] I. Chang, Finite element analysis of hepatic radiofrequency ablation probes using temperature-dependent electrical conductivity, Biomed. Eng. Online 2 (2003) 12.
[140] U. Zurbuchen, C. Holmer, K.S. Lehmann, T. Stein, A. Roggan, C. Seifarth, et al., Determination of the temperature-dependent electric conductivity of liver tissue ex vivo and in vivo: importance for therapy planning for the radiofrequency ablation of liver tumours, Int. J. Hyperther. 26 (2010) 26–33.
[141] S.R. Guntur, K.I. Lee, D.G. Paeng, A.J. Coleman, M.J. Choi, Temperature-dependent thermal properties of ex vivo liver undergoing thermal ablation, Ultrasound Med. Biol. 39 (2013) 1771–1784.
[142] R. Possebon, Y. Jiang, S. Mulier, C. Wang, F. Chen, Y. Feng, et al., A piecewise function of resistivity of liver: determining parameters with finite element analysis of radiofrequency ablation, Med. Biol. Eng. Comput. 56 (2018) 385–394.
[143] M. Reinhardt, P. Brandmaier, D. Seider, M. Kolesnik, S. Jenniskens, R. B. Sequeiros, et al., A prospective development study of software-guided radio-frequency ablation of primary and secondary liver tumors: clinical intervention modelling, planning and proof for ablation cancer treatment (ClinicIMPPACT), Contemp. Clin. Trials Commun. 8 (2017) 25–32.
[144] Z. Liu, M. Ahmed, Y. Weinstein, M. Yi, R.L. Mahajan, S.N. Goldberg, Characterization of the RF ablation-induced 'oven effect': the importance of background tissue thermal conductivity on tissue heating, Int. J. Hyperther. 22 (2006) 327–342.
[145] S.K. Hall, E.H. Ooi, S.J. Payne, A mathematical framework for minimally invasive tumor ablation therapies, Crit. Rev. Biomed. Eng. 42 (2014) 383–417.
[146] S.K. Hall, E.H. Ooi, S.J. Payne, Cell death, perfusion and electrical parameters are critical in models of hepatic radiofrequency ablation, Int. J. Hyperther. 31 (2015) 538–550.
[147] M. Jamil, E.Y. Ng, Quantification of the effect of electrical and thermal parameters on radiofrequency ablation for concentric tumour model of different sizes, J. Therm. Biol. 51 (2015) 23–32.
[148] O.S. Al-Kadi, D.Y. Chung, C.C. Coussios, J.A. Noble, Heterogeneous tissue characterization using ultrasound: a comparison of fractal analysis backscatter models on liver tumors, Ultrasound Med. Biol. 42 (2016) 1612–1626.
[149] H. Wi, A.L. McEwan, V. Lam, H.J. Kim, E.J. Woo, T.I. Oh, Real-time conductivity imaging of temperature and tissue property changes during radiofrequency ablation: an ex vivo model using weighted frequency difference, Bioelectromagnetics 36 (2015) 277–286.